XII International Conference on Computational Plasticity. Fundamentals and Applications
COMPLAS XII
E. Oñate, D.R.J. Owen, D. Peric and B. Suárez (Eds)

THE PHYSICAL AND NUMERICAL MODELING OF COLD WIRE DRAWING PROCESS OF BIOCOMPATIBLE MAGNESIUM ALLOYS

A. MILENIN*, P. KUSTRA* D. J. BYRSKA-WÓJCIK*

* AGH University of Science and Technology
Al. Mickiewicza 30, 30059 Krakow, Poland
e-mail: milenin@agh.edu.pl, www.lcm.agh.edu.pl

Key words: Wire drawing, boundary element method, magnesium alloys, fracture, multi-scale.

Summary. This paper is devoted to the new magnesium alloys used in medicine as a soluble implants. Feature of these alloys is a low technological ductility in cold forming. The problem of determination of the cold thin wire (diameter less than 0.1mm) drawing process parameters for hardly deformable biocompatible magnesium alloys by using the mathematical mesoscale model is described in the paper. In previous authors' works it is proven that the material state directly before forming the microcracks is the optimal state from the point of view of the restoration of plasticity by annealing. The forecasting of this material state in drawing process requires the development of the intergranular fracture initiation model and to use this model in two modes: - the modeling of the in-situ tests, what allows to calibration and validation of the model; - the modeling of the drawing process, what allows to optimize the drawing parameters. The developed model was implemented into authors' program Drawing2d, which is dedicated to drawing process. The results of mesoscale simulation were verified by using the experimental drawing process of the thin wires (diameter 0.07mm) following to developed technology. It was shown by analysis of microstructure that the model allows to forecast the microcracks initiation in the wire drawing process.

1 INTRODUCTION

The problem of the development of the drawing processes of magnesium alloys is related to their low technological plasticity [1-2]. This is applied to the most commercial alloys. Recently, the new magnesium alloys were developed containing supplements Ca, Li, Zn. These alloys are a good material for soluble implants [3-4] or surgical sutures [5-6]. Studies of the properties of these alloys showed that their technological plasticity during drawing is lower than commercial magnesium alloys [7-8]. In connection with this, there are some possibilities allowing increasing the plasticity of magnesium alloys during drawing.

1. Drawing at elevated temperatures in a hot die [9]. The advantage of this process is the lack of annealing operations between passes. This achieves high performance. For example, in [9] 25 passes of drawing process of Ax30 and MgCa08 alloys were performed to the wire diameter 0.1 mm with a total elongation 100 without using annealing between passes.

2. Drawing at room temperature with annealing between passes [6,10]. This approach requires strict control of the microstructure after each pass and performing annealing after one

or two passes. It is particularly important to prevent the occurrence of cracks at grain boundaries [10].

That's way an effective development of wire drawing process of magnesium alloys is possible only on the basis of a mathematical model that takes into account technological plasticity in the macro-scale, and changes in the structure of the material in the meso-scale. Existing approaches dedicated to modeling of fracture during drawing have limited applicability to the evaluation of technological plasticity magnesium alloys for the following reasons.

- Drawing process is the multi-pass cycle containing stage of deformation and annealing. It is not sufficiently to perform the fracture prediction in the current pass, as suggested by most of the existing models of metal fracture during drawing [2]. More importantly is to simulate changes occurring in the metal microstructure in the current pass and when will be effectively to restore ductility by annealing in this case.

- Feature of multi-pass process is that technological problems at current drawing pass not shows up immediately, but after next few passages. In this case, after the wire breakage is difficult to determine which of the early stages of technology contained errors.

In the papers [7-11] have been proposed to solutions of this problems at the meso and macro scales. However, these studies do not take into account the shear stress in the meso scale. Since the shear stress and strain significantly effect on plasticity, one of the goals of this work was to perform calculations in the micro scale, taking into account the shear deformations. The main purpose of this paper, however, is to numerical and physical modelling of the wire drawing of magnesium alloys in macro and meso scales.

2 MULTISCALE MODEL OF WIRE DRAWING

2.1 Macro-scale

The approach used in the simulation of wire drawing in macro-scale is based on solving coupled problems related to heat transfer and rigid-plastic deformation [11]. Solution of the mechanical problem obtained by using the FEM based following functional:

$$J = \int_V \int_0^{\bar{\xi}} \bar{\sigma}\left(\bar{\xi}, \bar{\varepsilon}, t\right) d\bar{\xi} dV + \int_V \sigma_0 \xi_0 dV - \int_F \sigma_\tau v_\tau dF - \int_F \sigma_n v_n dF \qquad (1)$$

where: $\bar{\sigma}$ – flow stress, σ_0 – mean stress, $\bar{\xi}$ – effective strain rate, ξ_0 – strain rate in the triaxial compression test, V – volume, F – contact surface, σ_τ – friction stress, v_τ – metal slip velocity with respect to the die.

Calculation for the boundary conditions in the dies belt has the features described in [12]. According to these studies, there is no possible to flow metal exactly along nominal working surface of dies during drawing process. Typically, the two phenomena distort the shape of the deformation - elastic deformation of dies and stripping material from the surface (undershoot). The developed solution offers a different solution to this problem, based on the method of penalty functions to satisfy the mechanical boundary conditions at the contact of metal with drawing dies. The proposed method is based on the modifications of functional (1), which described in papers [12,13].

The Saint-Venant-Levy-Mises theory is used for relation between stresses and strains rate

for plastic deformation:

$$\sigma_{ij} = \delta_{ij}\sigma_0 + \frac{2\overline{\sigma}}{3\overline{\xi}}\xi_{ij} \tag{2}$$

where: δ_{ij} – the Kronecker delta.

The flow stress of MgCa0.8 alloy was proposed as following function:

$$\overline{\sigma} = 230\overline{\varepsilon}^{0.08} \tag{3}$$

The tensor ε_{ij} is calculated by integration along the flow lines:

$$\varepsilon_{ij} = \int_0^{\tau} \xi_{ij}(\tau)d\tau = \sum_{m=1}^{m=m_\tau} \xi_{ij}^{(m)} \Delta\tau^{(m)} \tag{4}$$

where: $\Delta\tau^{(m)}$ – time increment, $\xi_{ij}^{(m)}$ – strain rate tensor determined according to equation:

$$\xi_{ij}^{(m)} = \sum_{n=1}^{n_{nd}} N_n \xi_{ijn} \tag{5}$$

where: N – finite element shape functions, ξ_{ijn} – nodal strain rate tensor for current finite element, n_{nd} – number of nodes in element.

The points of flow lines are determined on the basis of the values of the velocity at point m, which are calculated according to the formula:

$$v_i^{(m)} = \sum_{n=1}^{n_{nd}} N_n v_{in} \tag{6}$$

The calculation of the position of the next point (m+1) of flow line is carried out according to the equation:

$$x_i^{(m+1)} = x_i^{(m)} + v_i^{(m)}\Delta\tau \tag{7}$$

The solution of heat problem for the metal and die is described in [9]. Example of FE mesh used to solve the problems and solutions of the thermal problem in the metal and die is shown in Fig. 1. Integration along the flow lines was used to set the boundary conditions for the RVE. Fig. 1 shows two flow lines (line A and line B) along which the solution in the meso-scale was performed.

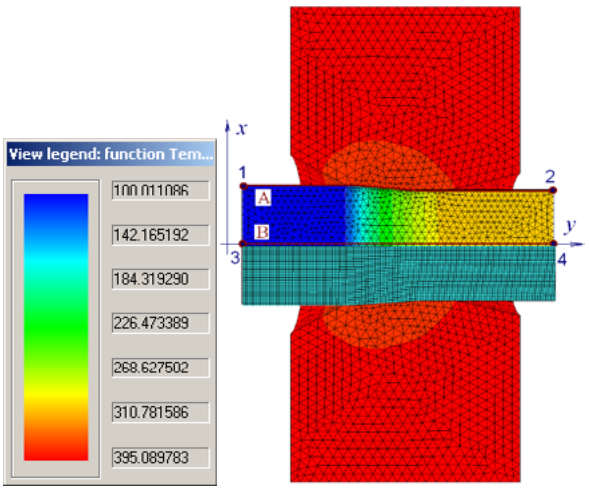

Figure 1: FE meshes involved in modeling of mechanical and thermal processes in die and wire, example of temperature distribution in the metal and die indicating flow lines along which the problem was solved in the meso-scale

2.2 Meso-scale

The developed model of fracture in the meso-scale was based on a preliminary in situ analysis of the fracture mechanism for a number of magnesium alloys. The experiments were performed at the Leibnitz Universität Hannover [14]. Results and technique of this experiment are presented in [7,14]. It is shown that these alloys, unlike typical magnesium alloys, fracture mainly on grain boundaries (Fig. 1) [7]. Therefore, long before the moment of fracture in macro-scale in the sample appears porosity. Fracture processes in this case were considered as simplified modeling of deformation within the grains. The scale of the model in this case will be called as mesoscopic (meso) scale. Because experimental studies [7, 14] showed that an intergranular fracture mechanism is mainly observed in the considered alloys, for practical application only the models in the macro- and meso-scales are examined.

In accordance with the observed fracture mechanism the follow assumptions were made to simplify the model in the meso-scale.

1. Assumed, that the fracture is only possible along the grain boundaries;
2. Used material model is the same as in the macro-scale;
3. The average characteristics of the stress and strain rates are considered in each grain. In this case, the material properties of grains can be linearized manner to that described in [7]. In the case of study of the problem at the micro-scale it can be used algorithms to better reflect the nonlinearity of the material [15-16].

The boundary element method (BEM) was selected as a basic method for solving the problem in the meso-scale. The advantages of this method, compared with the finite element method, applied to this problem described in [15-17].

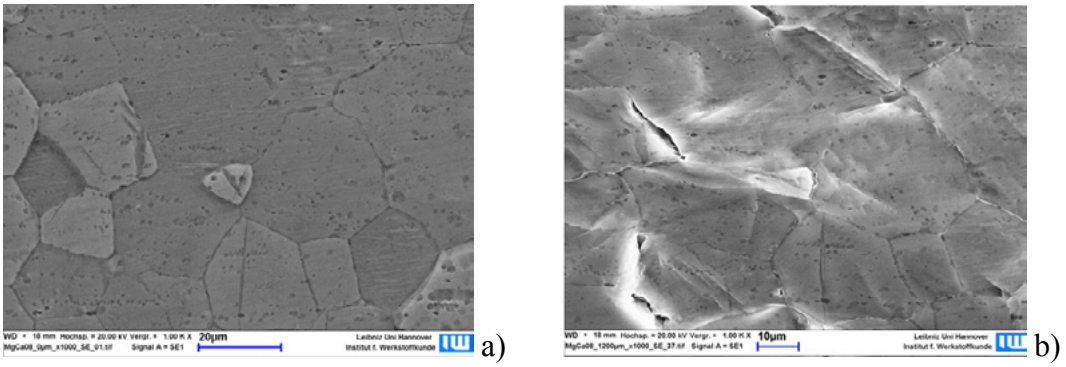

a) b)

Figure 2: The observed fracture of the MgCa0.8 alloy at various stages of tensile test: a - the initial microstructure, b - the propagation of cracks and an increase of porosity, elongation of the sample 1.2 mm.

Kelvin solution [17] for plane strain state and incompressible material $(\nu = 0.5)$ for single grain can be written as:

$$u_1 = \frac{3F_1}{2E_g}\left(g - x_1\frac{\partial g}{\partial x_1}\right) - \frac{3F_2x_2}{2E_g}\frac{\partial g}{\partial x_1}, \tag{8}$$

$$u_2 = \frac{3F_2}{2E_g}\left(g - x_2\frac{\partial g}{\partial x_2}\right) - \frac{3F_1x_1}{2E_g}\frac{\partial g}{\partial x_2}, \tag{9}$$

$$\sigma_1 = F_1\left(\frac{\partial g}{\partial x_1} - x_1\frac{\partial^2 g}{\partial x_1^2}\right) + F_2\left(\frac{\partial g}{\partial x_2} - x_2\frac{\partial^2 g}{\partial x_1^2}\right), \tag{10}$$

$$\sigma_2 = F_2\left(\frac{\partial g}{\partial x_2} - x_2\frac{\partial^2 g}{\partial x_2^2}\right) + F_1\left(\frac{\partial g}{\partial x_1} - x_1\frac{\partial^2 g}{\partial x_2^2}\right), \tag{11}$$

$$\sigma_{12} = F_2 x_2\frac{\partial^2 g}{\partial x_1 \partial x_2} - F_1 x_1\frac{\partial^2 g}{\partial x_1^2}, \tag{12}$$

$$g(x_1,x_2) = -\frac{1}{2\pi} ln\sqrt{(x_1^2 + x_2^2)}, \tag{13}$$

where: F_1 and F_2 are a force components, u_1, u_2 are displacements in the direction of the axis x_1 and x_2, σ_1, σ_2, σ_{12} are the stresses caused by the force F, E_g – elastic-plastic modulus of grain:

$$E_g = \frac{\bar{\sigma}_g(\bar{\varepsilon}_g)}{\bar{\varepsilon}_g} \tag{14}$$

To use the theory of plastic flow, equation (8) and (9) was differentiated by time:

$$v_1 = \frac{3F_1}{2\mu_g}\left(g - x_1\frac{\partial g}{\partial x_1}\right) - \frac{3F_2 x_2}{2E}\frac{\partial g}{\partial x_1}, \tag{15}$$

$$v_2 = \frac{3F_2}{2\mu_g}\left(g - x_2\frac{\partial g}{\partial x_2}\right) - \frac{3F_1 x_1}{2E}\frac{\partial g}{\partial x_2}, \tag{16}$$

where :

$$\mu_g = \frac{\bar{\sigma}_g(\bar{\varepsilon}_g)}{\bar{\xi}_g}. \tag{17}$$

The algorithm for calculating the mean values of the stress-strain parameters in the grains is described in [7].

The Saint-Venant-Levy-Mises theory is used for relation between stresses and strain rates for plastic deformation:

$$\sigma_{ij} = \delta_{ij}\sigma_0 + \frac{2}{3}\mu_g\xi_{ij} \tag{18}$$

where σ_0 – the mean stress in grain, ξ_{ij} – strain rate tensor in grain.

Calculating of the heterogeneous grain orientation microstructure is performed based on data on the orientation of crystals of magnesium after extrusion [18-20]. Used effective value of the yield stress of the grain [21], and the effective viscosity of the material grain:

$$\bar{\sigma}_g(\bar{\varepsilon}) = k_g\bar{\sigma}_{grain}(\bar{\varepsilon}) \tag{19}$$

$$\bar{\mu}_g = k_g\frac{\bar{\sigma}_g(\bar{\varepsilon}_g)}{\bar{\xi}_g} \tag{20}$$

The coefficient k_g for each grain is set based on the random grain orientation in the range of 0.81-1.19.

The boundary element mesh is generated (Fig. 3), consisting of zones, that simulate the grain to use the BEM, based on photographs of the original microstructure [22]. The boundary conditions for the representative volume element (RVE) are defined based on the simulation results in the macro-scale for any flow line. In the direction of wire drawing the deformation ε_y is set, and in the direction perpendicular to the wire axis defined stress σ_x. Since the shear stress and strain significantly effect on plasticity [23], the shear deformation ε_{xy} is taken into account by setting the relevant incremental displacements on the boundary of RVE.

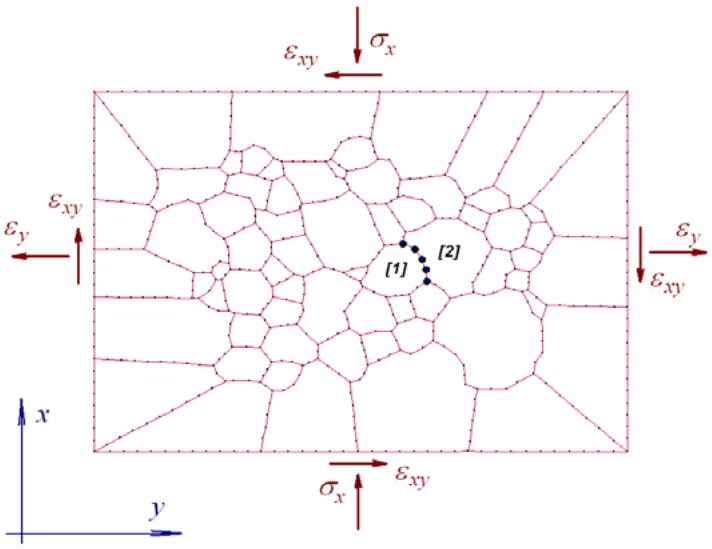

Figure 3: An example of a digital representation of a fragment of the microstructure and the boundary condition

Conditions of continuity of the grain boundaries (grain shown for 1 and 2 in Fig. 3.)were used at the initial stage of deformation :

$$\sigma_s^{[1]}\left(x_q,y_q\right)=\sigma_s^{[2]}\left(x_q,y_q\right), \tag{21}$$

$$\sigma_n^{[1]}\left(x_q,y_q\right)=\sigma_n^{[2]}\left(x_q,y_q\right), \tag{22}$$

$$v_s^{[1]}\left(x_q,y_q\right)=-v_s^{[2]}\left(x_q,y_q\right), \tag{23}$$

$$v_n^{[1]}\left(x_q,y_q\right)=-v_n^{[2]}\left(x_q,y_q\right), \tag{24}$$

where: $\sigma_s^{[1]}\left(x_q,y_q\right)$, $\sigma_n^{[1]}\left(x_q,y_q\right)$ are the shear and normal components of stress from grain 1 and $\sigma_s^{[2]}\left(x_q,y_q\right)$, $\sigma_n^{[2]}\left(x_q,y_q\right)$ are the shear and normal components of stress from grain 2 in point q. The same notation is applied to velocities. When the failure criterion is satisfied on the boundary, these conditions for a given pair of boundary elements are excluded.

Fracture criterion based on the approach described in [10, 24-25] was applied. In comparison to these works, the criterion was modified by replacing the integration over time to integration over RVE deformation:

$$D=\int_0^{\varepsilon_{ijRVE}} b_1\left(\frac{\sigma_{eq}}{E}\right)^{b_2}\left(1-D\right)^{b_3} d\varepsilon_{ijRVE}\le 1 \tag{25}$$

$$\sigma_{eq}=\sqrt{\sigma_n^2+b_0\sigma_S^2}, \tag{26}$$

where: σ_n is positive part of the normal stress, σ_s is the shear stress, E is Young's modulus, and b_0-b_3 are empirical parameters.

This is related to the low sensitivity of the material strain rate, which makes the procedure time integration used in [10] low effective.

Calibration and validation of the model in the meso-scale was described in [14]. Calibration of this model is made by the determination of the coefficients b_0-b_3 by minimizing the objective function G, based on the difference between the porosity of the microstructure

obtained in the experiments in situ γ_i^{exper} and the results of calculation γ_i^{calc} (δ_1) and takes into account the time of first occurrence of cracks at grain boundaries (δ_2):

$$\delta_1 = \sum_{i=1}^{N_{incr}} \left(\gamma_i^{calc} - \gamma_i^{exper}\right)^2 \tag{27}$$

$$\delta_2 = \left(\tau^{calc} - \tau^{exper}\right)^2 \tag{28}$$

$$G = w_1\delta_1 + w_2\delta_2 \tag{29}$$

where: w_1, w_2 - weights of components of the objective function G.

Figure 4 show the results of simulation of tests in situ for the conditions corresponding to the data presented in Figure 2b. The empirical coefficients obtained from the calibration were the following b_1=27; b_2=0.3; b_3 = -0.5; b_0=0.4.

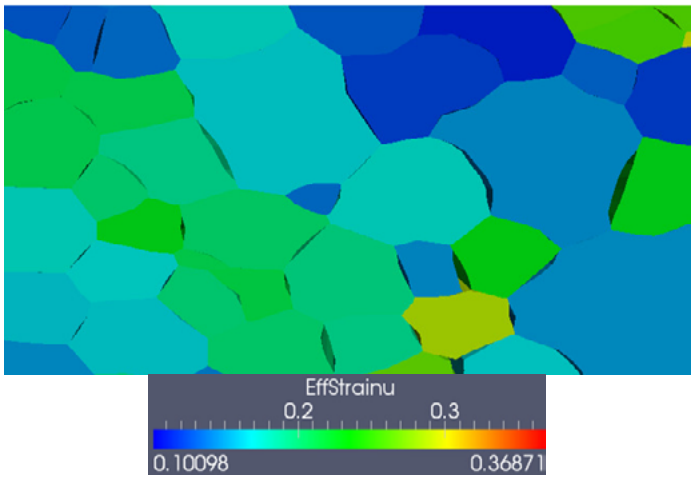

Figure 4: The results of simulation for experiments of in situ tensile for elongation 1.2 mm.

3. PHYSICAL MODELLING IN MESO-SCALE AND VALIDATION OF NUMERICAL MODEL

For the purpose of validation of the proposed techniques two variants of physical modeling of wire drawing in laboratory conditions [10] were proposed:

variant 1: elongation per pass 1.096;

variant 2: elongation per pass 1.20.

The angle in each pass was 5^0. Speed of drawing was 10 mm/s and was chosen in such a way that could enable annealing in a furnace installed before the device for drawing. All passages in each variant were geometrically similar, so for calculated results of stress and strains all passageways are close. Therefore, only simulation of the first passage for each variant was performed.

Figure 5 shows the results of simulation of the first pass for variant 1: Fig.5a - distribution of ε_{xy}; Fig.5b - σ_x; Fig.5c - ε_y. Analogical data for variant 2 are presented on Fig. 6.

Those data are used to define boundary conditions for RVE in accordance with the scheme in Fig. 3.

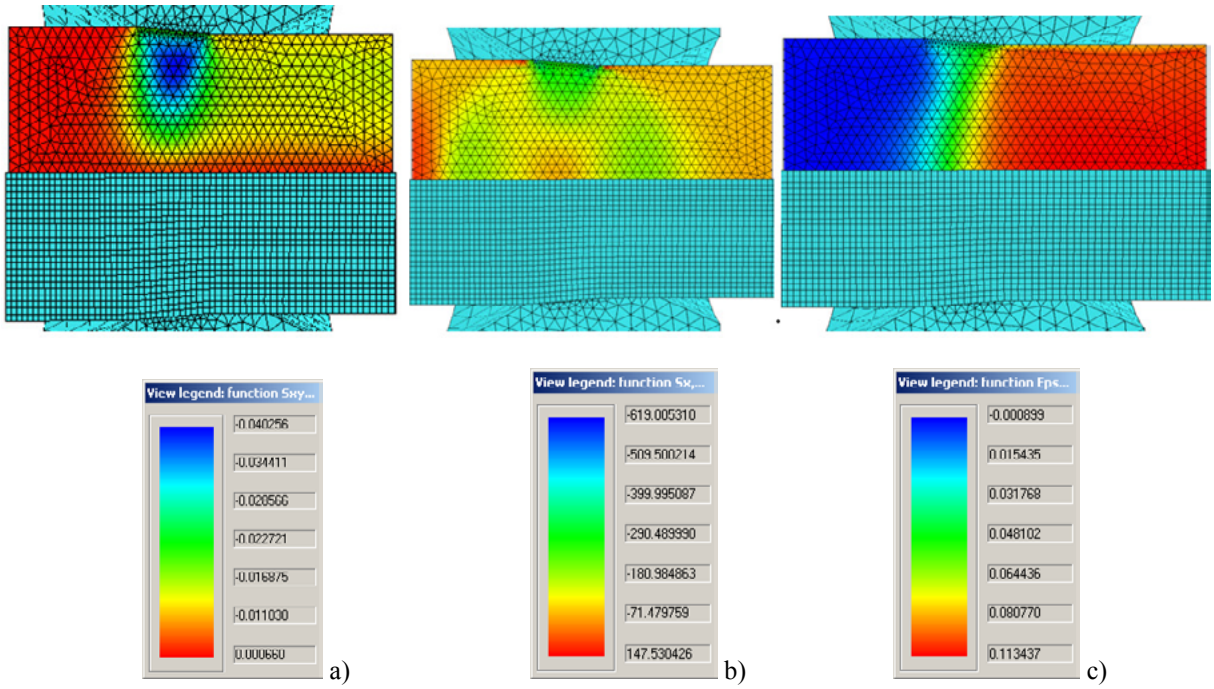

Figure 5: Results of simulation of the first pass for variant 1: a - distribution of ε_{xy} ; b - σ_x ; c - ε_y .

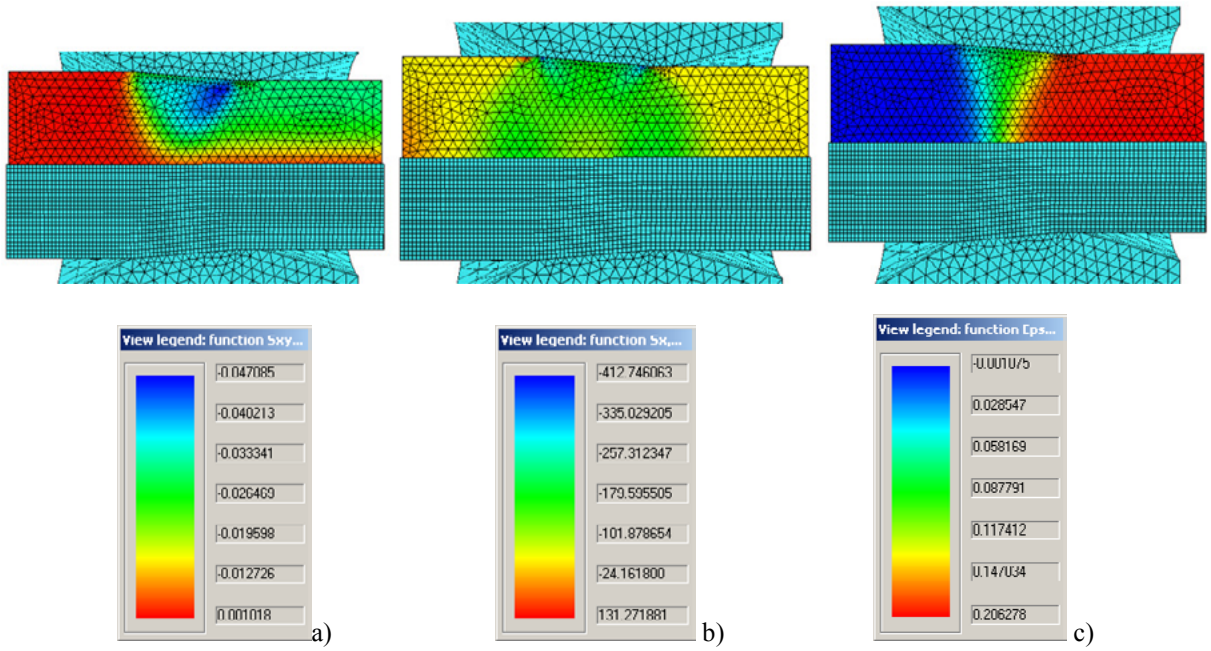

Figure 6: Results of simulation of the first pass for variant2: a - distribution of ε_{xy} ; b - σ_x ; c - ε_y

Calculations in meso-scale have been executed for each considered variants for the surface and central line of wire (the flow lines A and B on the Fig.1a). The results are presented for the final stage of deformation in Fig.7 (variant 1) and Fig.8 (variant 2).

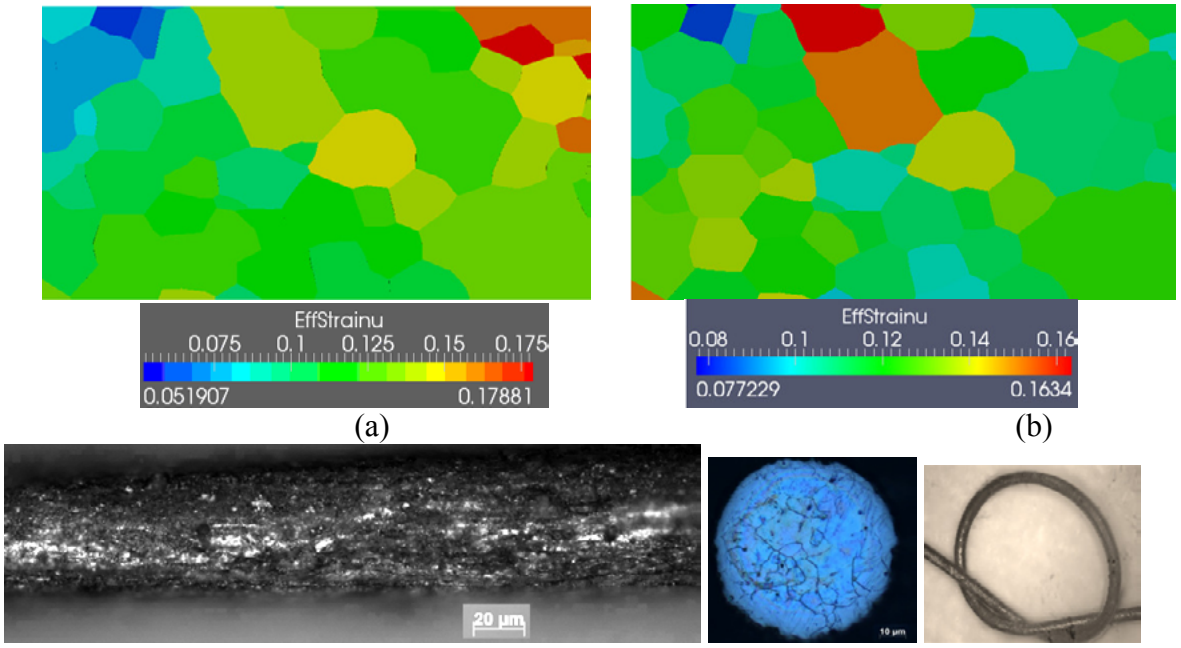

Figure 7: Wire d=0.0758 mm after drawing according to variant 1 (a – surface, simulation, b – centerline, simulation, c-e - experiment).

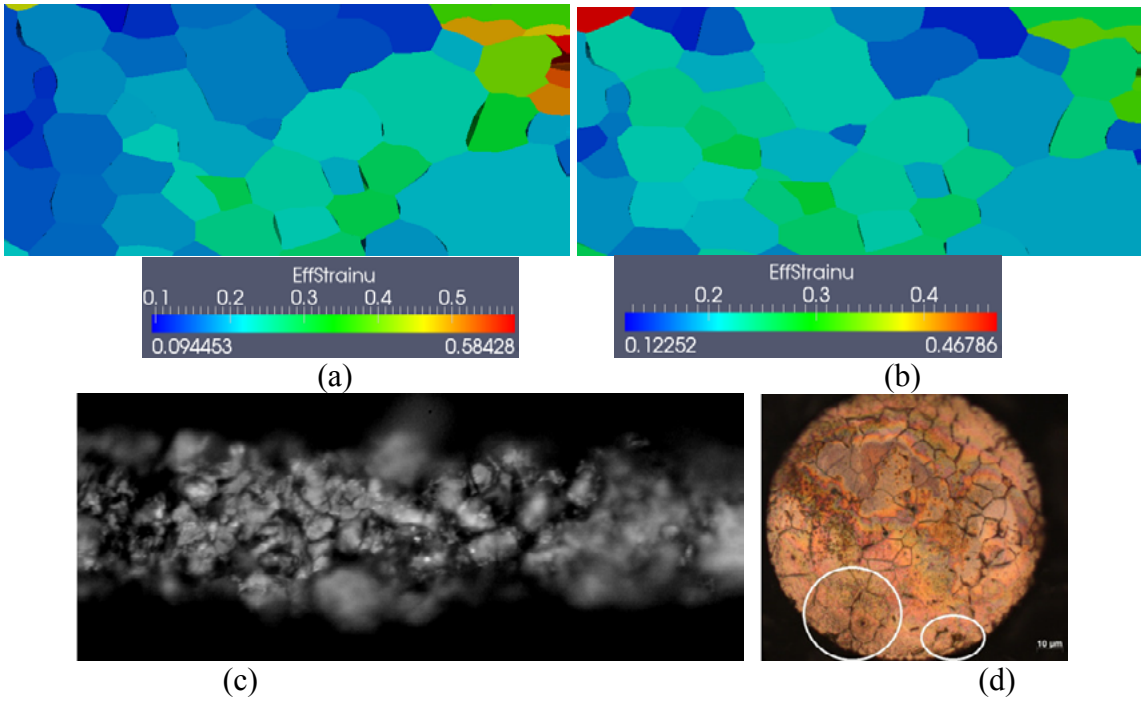

Figure 8: Network of cracks after the 4th passage d=0.112 mm, variant 2 (a – surface, simulation, b – centerline, simulation, c-d - experiment).

From the obtained data it is follows that in variant 1 in center line of wire is not cracks on

the grain boundaries (Fig. 7). On the surface, however, the calculation shows the appearance of a small number of cracks (Fig. 7b). This is due to the action of shear and tensile stresses in the surface of wire in calibration belt. The experiment was carried out for the calculation conditions, it has shown good results, cracks after 4 passes are not detected (Fig. 7c, 7d). The resulting wire had good ductility (Fig. 7e). In the variant 2 only 4 passage were possible. After passage number 2 a hairline fractures on the borders of grains (Fig.8) on the surface of the wire can be observed using an optical microscope. Obtained wire was fragile and crumbles when trying to tie a knot after the second pass. Fig.8c,d show a developed network of cracks after 4 passages. Further attempts of annealing and drawing were unsuccessful. By using variant 1 of the drawing the wire with much higher quality was obtained, mechanical properties of obtained wire allow further drawing.

4 CONCLUSIONS

It is shown that the application of multiscale modeling allows solving the problem of the development of technological modes of wire drawing for magnesium alloys. The developed computer code is based on the FEM for the macro-scale and BEM for the problem in the meso-scale. Prediction of the initiation of fracture using multiscale model coincided with the results of the experiment. Based on the developed schedule it was possible to get the wire with diameter 0.0758 mm from Ax30 alloy by cold drawing.

REFERENCES

[1] Odawa N., Shiomi M., Osakada K.: Forming limit of magnesium alloy at elevated temperatures for precision forming, *Int. J. of Machine Tools & Manufacture*, (2002), 42, 607-614.

[2] Yoshida K., Cold drawing of magnesium alloy wire and fabrication of microscrews. *Steel Grips*, 2, (2004), 199-202.

[3] Haferkamp H., Kaese V., Niemeyer M., Phillip K., Phan-Tan T., Heublein B., Rohde R.: Exploration of magnesium alloys as new material for implantation. *Mat.-wiss. u. Werkstofftech*, 32: Wiley-VCH Verlag GmbH, Weinheim, (2001), 116-120.

[4] Thomann M., Krause Ch., Bormann D., N. von der Hoh, Windhagen H., Meyer-Lindenberg A.: Comparison of the resorbable magnesium alloys LAE442 and MgCa0.8 concerning their mechanical properties, their progress of degradation and the bone-implant-contact after 12 months implantation duration in a rabbit model, *Mat.-wiss. u. Werkstofftech* (2009), 40, No1-2.

[5] A. Milenin, P.Kustra, J.-M.Seitz, F.-W.Bach, D.Bormann Production of thin wires of magnesium alloys for surgical applications. *Wire Journal International* (2011), Vol. 44 Issue 6, p. 74.

[6] Seitz, J.-M., Wulf, E., Freytag, P., Bormann, D. and Bach, F.-W., The Manufacture of Resorbable Suture Material from Magnesium. *Advanced Engineering Materials*, (2010) 12: 1099–1105. doi: 10.1002/adem.201000191

[7]A. Milenin, D. Byrska, O. Gridin The multi-scale physical and numerical modeling of fracture phenomena in the MgCa0.8 alloy. *Computers and Structures*, (2011), 89, 11–12, 1038–1049, doi:10.1016/j.compstruc.2011.01.003

[8] A. Milenin, D. J. Byrska, O. Grydin, M. Shaper, The experimental research and the

numerical modeling of the fracture phenomena in micro scale. *Computer Methods in Materials Science*, (2010), vol. 10, no. 2, p. 61–68.
[9] Milenin A., Kustra P. Numerical and experimental analysis of wire drawing for hardly deformable biocompatible magnesium alloys. *Archives of Metallurgy and Materials*, (2013), Vol 58, p. 55-62, doi:10.2478/v10172-012-0150-0
[10] A. Milenin, P. Kustra, D. J. Byrska-Wójcik The physical and numerical mesoscale modeling of cold wire drawing process of hardly deformable biocompatible magnesium alloys. *Archives of Metallurgy and Materials*, (2012), vol. 57, 4, p. 1117-1126, doi:10.2478/v10172-012-0125-1
[11] A. Milenin, Program komputerowy Drawing2d – narzędzie do analizy procesów technologicznych ciągnienia wielostopniowego. *Hutnik-Wiadomości Hutnicze*, (2005), 72, 100-104.
[12] S.Shirasaki, M.Asakawa, R.Komami, Y.Tanaka Theoretical Analysis of High Dimensional Accuracy in Cold Wire Drawing // *Steel Research Int.* 81 (2010), No 9, P. 494-497
[13] A. Milenin, F. Grosman, L. Madej, and J. Pawlicki FEM simulation of rolling process with cyclic horizontal movement of rolls. *Steel Research Int.* 81 (2010), 3, P. 204-209, doi: 10.1002/srin.200900094.
[14] A. Milenin, D. J. Byrska-Wójcik, O. Grydin, M. Schaper The physical and numerical modeling of intergranular fracture in the {Mg-Ca} alloys during cold plastic deformation // *W: Metal Forming 2012: proc. 14th int. conf.:* September 16–19, 2012, Krakow, Poland/ eds. Jan Kusiak, Janusz Majta, Danuta Szeliga. - Weinheim : Wiley-VCH Verlag GmbH & Co. KGaA, cop. 2012. — (Steel Research International; spec. ed.). P. 863–866.
[15] G. K. Sfantos, M. H. Aliabadi: A boundary cohesive grain element formulation for modeling intergranular microfracture in polycrystalline brittle. *Int. J. Numer. Meth. Engng*, 69 (2007), 1590–1626.
[16] G. K. Sfantos, M. H .Alibadi Multi-scale boundary element modeling of material degradation and fracture, *Computer Methods in Applied Mechanics and Engineering*, 196, 2007, 1310-1310.
[17] S.L. Crouch, A.M. Starfield, *Boundary element methods in solid mechanics*, GEORGE ALLEN & UNWIN 1983, London, Boston, Sydney.
[18] T. Mayama, T. Ohashi, K. Higashida, Y. Kawamura Crystal plasticity analysis on compressive loading of magnesium with suppression of twinning. *Magnesium Technology* 2011 Edited by: Wim H. Sillekens, Sean R. Agnew, Neale R. Neelameggham, and Suveen N. Mathaudhu . -TMS (The Minerals, Metals & Materials Society), (2011) P. 273-277
[19] T. Mayama, K. Aizawa, Y. Tadano, M. Kuroda Influence of twinning deformation and lattice rotation on strength differential effect in polycrystalline pure magnesium with rolling texture. *Computational Materials Science* 47 (2009) 448–455.
[20] Mayama, T., et al. Crystal plasticity analysis of texture development in magnesium alloy during extrusion. *Int. J. Plasticity* (2011), doi:10.1016/j.ijplas.2011.02.007
[21] L. Madej *Development of the Modelling Strategy for the Strain Localization Simulation Based on the Digital Material Representation* // AGH University of Science and Technology, Krakow, Vol. 221, 2010.
[22] Ł. Rauch, K. Bzowski Image processing methods for segmentation of microscopic

pictures of the {MgCa} alloys, *Computer Methods in Materials Science*, (2011), 11, 2, 350–356.
[23] Bao Y, Wierzbicki T. On fracture locus in the equivalent strain and stress triaxility space. *International Journal of Mechanical Sciences*. (2004); 46:81–98.
[24] L.M. Kachanov, On the time to failure under creep conditions, *Izv. Akad. Nauk. SSSR*, Otd. Tekhn. Nauk. 8 (1958) 26–31.
[25] O. Diard, S. Leclercq, G. Rousselier, G. Cailletaud, Distribution of normal stress at grain boundaries in multicrystals: application to an intergranular damage modeling, *Computational Materials Science*, 18, (2002) 73-84.

Acknowledgements: Financial assistance from the Ministry of Science and high Education of Poland, project AGH no. 11.11.110.150 is acknowledged.